Phenotypic Knockout of Nerve Growth Factor in Adult Transgenic Mice Reveals Severe Deficits in Basal Forebrain Cholinergic Neurons, Cell Death in the Spleen, and Skeletal Muscle Dystrophy

Francesca Ruberti,[1] Simona Capsoni,[1] Alessandro Comparini,[2] Elena Di Daniel,[1] Jessica Franzot,[1] Stefania Gonfloni,[1] Gabriella Rossi,[1] Nicoletta Berardi,[2] and Antonino Cattaneo[1]

[1]Neuroscience Program, International School for Advanced Studies (SISSA), 34014 Trieste (Italy), and [2]Consiglio Nazionale delle Ricerche, Institute of Neurophysiology, 56100 Pisa, Italy

The disruption of the nerve growth factor (NGF) gene in transgenic mice leads to a lethal phenotype (Crowley et al., 1994) and hinders the study of NGF functions in the adult. In this study the phenotypic knockout of NGF in adult mice was achieved by expressing transgenic anti-NGF antibodies, under the control of the human cytomegalovirus promoter. In adult mice, antibody levels are 2000-fold higher than in newborns. Classical NGF targets, including sympathetic and sensory neurons, are severely affected. In the CNS, basal forebrain and hippocampal cholinergic neurons are not affected in the early postnatal period, whereas they are greatly reduced in the adult (55 and 62% reduction, respectively). Adult mice show a reduced ability in spatial learning behavioral tasks. Adult, but not neonatal, transgenic mice further show a new phenotype at the level of peripheral tissues, such as apoptosis in the spleen and dystrophy of skeletal muscles. The analysis of this novel comprehensive transgenic model settles the controversial issue regarding the NGF dependence of cholinergic neurons in adult animals and reveals new NGF functions in adult non-neuronal tissues. The results demonstrate that the decreased availability of NGF in the adult causes phenotypic effects via processes that are at least partially distinct from early developmental effects of NGF deprivation.

Key words: adult transgenic mice; neurotrophins; cholinergic deficits; behavioral impairment; muscular dystrophy; apoptosis; spleen

The nerve growth factor (NGF) (Levi-Montalcini, 1952) is required for the differentiation and/or the survival of specific neuronal populations during development, including sensory, sympathetic, and basal forebrain cholinergic neurons (BFCNs) (Levi-Montalcini, 1987). NGF also exerts actions on non-neuronal cell populations (Levi-Montalcini, 1987). After the early use of anti-NGF antibodies (Levi-Montalcini and Booker 1960), NGF functions *in vivo* have been investigated with different approaches, including the systemic (Levi-Montalcini and Angeletti, 1966; Gorin and Johnson, 1979, 1980) or local (Li et al., 1995; Van der Zee et al., 1995; Molnar et al., 1998) delivery of anti-NGF antibodies and the disruption of the NGF gene in transgenic mice (Crowley et al., 1994). The ablation of NGF function gives rise to a lethal phenotype in the early postnatal period, preventing the analysis of NGF function in adult animals. On the other hand, adult heterozygous NGF knockout mice (*ngf*+/−) show only a mild cholinergic phenotype and no other described deficits (Chen et al., 1997). No comprehensive transgenic model allowing the study of the pleiotropic actions of NGF in adult mice is currently available. Given the potential clinical relevance of some of the described actions of NGF, the lack of such a model represents a severe limitation.

After the demonstration that recombinant antibodies can be efficiently secreted by cells of the nervous system (Cattaneo and Neuberger, 1987), a novel approach for phenotypic knockout (the neuroantibody approach) has been proposed and validated (Piccioli et al., 1991, 1995).

In this study we generated transgenic mice expressing a recombinant version of a neutralizing anti-NGF monoclonal antibody (mAb αD11) (Cattaneo et al., 1988; Ruberti et al., 1993). Phenotypic analysis of sympathetic, sensory, and cholinergic neurons showed that the neutralization of NGF in adult transgenic mice is extremely effective. This analysis also revealed a severe dystrophy in skeletal muscles and a massive cell death in the spleen of adult mice. The study of this novel comprehensive transgenic model uncovered new functions of NGF, broadening the spectrum of its biological activities.

MATERIALS AND METHODS

Production of transgenic mice. The plasmids pcDNAI-neo/VKαD11HuCK and pcDNAI-neo/VHαD11HuCγ, carrying the light and heavy chain genes, respectively, of the chimeric antibody αD11 (Ruberti et al., 1993) under the transcriptional control of the human cytomegalovirus (CMV) early region promoter [−601 to −16 (Boshart et al., 1985)], were digested with *Kpn*I–*Apa*LI and *Kpn*I–*Xba*I, respectively, to isolate the transcriptional units. The fragments were microinjected in the pronucleus of single-cell fertilized C57BL/6 × SJLF2 hybrid mouse eggs, either individually or in combination, and the injected eggs were reintroduced into foster pseudopregnant females of an outbred strain different from that of the microinjected eggs. Production of transgenic mice was performed by a custom transgenic service (DNX Corporation, Princeton, NJ). Analysis

Received Sept. 23, 1999; revised Jan. 20, 2000; accepted Jan. 26, 2000.

We dedicate this paper to Rita Levi-Montalcini.

We are grateful to Kevin Ainger, Silvia Biocca, and Luciano Domenici for critically reading this manuscript and for useful comments. We are indebted to Katia Gamel, Patrizia Piccioli, Massimo Righi, and Anna Rosati for technical help during different phases of the work. We thank Cristina Bottin, Sabina Giannotta, and Mauro Melato (University of Trieste) for help with the flow cytometry. The invaluable help of Marco Stebel with the management of the colony is gratefully acknowledged.

F.R. and S.C. contributed equally to this paper.

Dr. Ruberti's and Dr. Gonfloni's present address: European Molecular Biology Laboratories (EMBL), Meyerhofstrasse 1, 69117 Heidelberg, Germany.

Correspondence should be addressed to Antonino Cattaneo, Neuroscience Program, International School for Advanced Studies (SISSA), Via Beirut 2/4, 34014 Trieste, Italy. E-mail: cattaneo@sissa.it.

 0270-6474/00/202589-13$15.00/0

of transgenic mice was performed by PCR and dot blot, on genomic DNA from tail biopsies, as described (Piccioli et al., 1995). For the dot blot, the heavy chain probe was a *Bam*HI–*Xba*I fragment from pcDNAI-neo/VHαD11HuCγ, encompassing the human heavy chain constant region, whereas the light chain probe was a *Bam*HI–*Apa*LI fragment isolated from plasmid pcDNAI-neo/VKαD11HuCK, encompassing the human light chain constant region. The DNA was quantitated by optical density at 260 nm before loading on the filter.

Two founder mice with the light chain transgene, two with the heavy chain transgene, and three double transgenic mice were generated, but despite an intensive breeding program, no offspring were generated.

Mice homozygous for the αD11 heavy chain transgene (VH-αD11 mice, lines C and D) and mice homozygous for the αD11 light chain transgene (VK-αD11 mice, lines A and B) were generated from the corresponding founders, by at least two crossings. Homozygosity was verified by genomic PCR analysis on offspring obtained by crossing putative homozygous to negative mice (at least two independent litters for each homozygous line). To obtain mice expressing both chains, and thus reconstituting NGF binding activity, single transgenic mice were intercrossed in different combinations (see Table 1).

Two groups of controls were used for the phenotypic analysis of family 1 and family 2 mice: wild-type mice and the corresponding single transgenic controls, expressing only the VH-αD11 heavy chain (C or D, as appropriate; see Table 1).

RNA analysis. Total RNA was isolated by the guanidine-isothiocyanate procedure (Chomcynzski and Sacchi, 1987) and analyzed by RNase protection. The size of the expected protected band was 340 bp for VH and 310 bp for VK. The template for β-actin mRNA transcription was a *Rsa*I, 1700 bp fragment in pGEM4Z. Transcription with T7 polymerase produced a 110 bp probe. VH, VK, and β-actin antisense RNA probes were hybridized to 20 μg of RNA in 80% formamide (46°C for 12–16 hr) and treated with RNase A and T1. Protected fragments were electrophoresed through a 4–6% acrylamide, 8 M urea gel and autoradiographed.

Anti-NGF antibody detection in blood serum and brain. Levels of recombinant αD11 antibody were detected in the blood serum and brain of adult mice by means of ELISA as described (Molnar et al., 1998), using a secondary anti-human IgG biotinylated antibody. Tissue extracts from brain were prepared as described (Piccioli et al., 1995). The amounts of recombinant antibody found in the serum and in the brain were determined by comparison to a calibration curve. Purified αD11 antibody dilutions were prepared, in the range between 0.125 and 250 ng of purified αD11, in 2% milk/PBS containing 1:10 dilutions of blood serum or brain extracts, as appropriate. Blood serum and brain extracts from transgenic mice were diluted 1:10 in 2% milk/PBS and used for ELISA.

Determination of free NGF. The levels of free NGF (i.e., NGF not bound to the transgenic antibodies) in the different tissues were determined by an ELISA assay. This assay exploits the property of αD11 antibody to recognize NGF in a two-site ELISA format (Gonfloni, 1995). Samples of blood serum or of tissue extracts [derived as in Molnar et al. (1998)] were added to wells coated with mAb αD11 (coating concentration of 5 μg/ml). After incubation for 2 hr at room temperature and extensive washing with PBS–0.05% Tween 20 followed by PBS, free NGF, not engaged with transgenic αD11, was detected using an affinity-purified rabbit anti-NGF polyclonal antiserum.

Histochemistry. Adult (2 months old) transgenic controls and anti-NGF mice were anesthetized with 10.5% chloral hydrate/saline (8 μl/g body weight) and then transcardially perfused with 4% paraformaldehyde in PBS. Organs were removed, post-fixed for 2 hr at 4°C, cryoprotected in 20% sucrose overnight, and then frozen in isopentane at −20°C. Coronal sections (14 μm thick) were collected on gelatin-coated slides, preincubated in 10% fetal calf serum and 5% bovine serum albumin, and processed for detection of different antigens using avidin–biotin alkaline phosphatase or horseradish peroxidase Elite Standard kits (Vector laboratories, Burlingame, CA). Biotinylated anti-human heavy chain (Amersham, Arlington Heights, IL) and anti-human light chain (Amersham or Vector) were used as primary antibodies at 1:500 and 1:50, respectively. For phenotypic analysis, the following primary antibodies were used: anti-choline acetyl transferase (ChAT; Chemicon, Temecula, CA) 1:200, anti-TrkA (mouse monoclonal MNAC13) 1:100, anti-p75 and anti-calcitonin gene-related peptide (CGRP; Roche Diagnostics, Mannheim, Germany) 1:10, anti-TrkB (Santa Cruz, Santa Cruz, CA) 1:200, anti-substance P [SP, monoclonal antibody NC1/34HL, (Cuello et al., 1979)] 1:200, and anti-tyrosine hydroxylase (TH; Chemicon) 1:100. Parallel sections from transgenic and age-matched transgenic control (VH only) mice were collected on the same slide. Alternate serial sections were incubated with primary antibodies or stained with cresyl violet or hematoxylin/eosin.

To detect the coexpression of the heavy and light chain of the transgenic antibody, sections were incubated first with biotinylated anti-human heavy chain antibodies. After the development of the reaction with avidin fluorescein (FITC) conjugate (Sigma, St. Louis, MO) and extensive washes, sections were incubated with biotinylated anti-human light chain antibodies. The labeling was evidentiated with avidin tetramethylrhodamine isothiocyanate (TRITC) conjugate (Sigma).

A Timm's staining protocol described by Wenzel et al. (1997) was used to label mossy fibers of hippocampus. Apoptotic cells were revealed with the *In Situ* Cell Death Detection Kit (Roche Diagnostics). For the double-labeling, fluorescein-labeled dUTP and an extravidin–TRITC conjugate (Sigma) were used to detect apoptotic and heavy and light chains, respectively.

For each morphological analysis, a mean number of six transgenic control and six anti-NGF mice were used. Cholinergic neurons of the basal forebrain and the hippocampus were counted, in 40 μm sections, with a 200× magnification at four representative levels indicated by Franklin and Paxinos (1997) (from bregma 1.32 mm to bregma 0.38 mm through the rostrocaudal extension of the basal forebrain and from bregma −2.75 mm to bregma −2.92 of the hippocampus). One of every six sections was taken into consideration. In each section only cells showing a clear nucleus were counted. For each group of animals the mean number of cells/mm^2 was calculated. Unpaired *t* test was performed to evaluate the statistical significance.

The number of neurons of dorsal root ganglia (DRG) and superior cervical ganglia (SCG) was evaluated on 10 μm coronal sections counterstained with cresyl violet. One section every three, throughout the extension of the ganglia, was analyzed. Only neurons with nucleus and nucleoli were counted, with a 400× magnification. For DRG, the fourth and fifth lumbar ganglia were analyzed.

Cell size histograms for DRG, SCG, and skeletal muscles were determined using a Zeiss microscope connected to a video camera and the image analysis program OPTIMAS 6.1 (Optimas Corporation, Bothell, WA). The same equipment was used to analyze the cross-sectional area of the middle section (the section of maximum diameter) of SCG.

Quantitative stereology. Anatomical boundaries used to define the basal forebrain were the corpus callosum, for the dorsal aspect, the ventral surface of the brain, and, laterally, a line passing medial to the rostral limb of the anterior commissure. The rostral boundary was determined by a plane passing through the rostral genu of the corpus callosum, and the caudal boundary was coincident with a plane passing through the first section containing the anterior commissure. The diagonal band nucleus was distinguished from the medial septum using a plane passing ventral to the rostral limb of the anterior commissure. All anatomical references were taken from Franklin and Paxinos (1997). The volume of the BF was calculated using the method of Cavalieri, as described previously (Michel and Cruz-Orive, 1988; Peterson et al., 1999). Briefly, a point-counting grid was superimposed over the video monitor on which the basal forebrain was displayed using a 2.5× objective. A volume probe was obtained by multiplying the distance between sections (*T*) and the area per point (*a*/*p*). The total volume (V_{ref}) was obtained by counting the number of points (P_i) overlying the BF in semiserial sections (one in six) sections and multiplying that sum by the volume associated with each point, according to the formula $V_{ref} = (\Sigma P_i)(a/p)\ (T)$.

Estimation of the total number of ChAT-positive neurons was achieved using the optical fractional method (West, 1993; Peterson et al., 1999). High resolution images (60×) were acquired on a Zeiss microscope equipped with a CCD camera and displayed by using the Optimas 6.1 analysis program. The numerical density (N_v) was determined by placing an unbiased counting frame on the monitor screen corresponding to the brain region. The number of neurons in the frame (of known area) were counted by focusing on the tissue at a known distance (20 μm), according to Sterio (1984). The number of cells in this volume yields a number of cells/volume (N_v), which is averaged over the entire sampled region. The total number of neurons was calculated by multiplying N_v by the total estimated volume of the BF region (known from the Cavalieri procedure). Volume and total number of ChAT positive-cells were evaluated using three animals for each group. Statistical analysis was performed using a two-tail *t* test.

Flow cytometry. For flow cytometric analysis, red cells were removed from dissociated spleens by lysis. Splenocytes were incubated with primary antibodies [FITC-labeled anti-mouse IgG (1:50, Sigma), IgM (1

μg/100 μl), IgD (1 μg/100 μl), and IgA (2 μg/100 μl) (PharMingen, San Diego, CA)] for 30 min at 4°C and analyzed with a Coulter Epics Elite Esp Flow Cytometer (Coulter Corporation, Miami, FL) at 488 nm.

Behavioral tests. The nociceptive hot plate test was as described (Eddy and Leimbach, 1953). The latency times for licking of the hind paws and for jumping were 30 and 240 sec, respectively.

For spatial learning, mice were tested in a standard eight-arm radial maze, placed in a quiet, well lit room, with many extra-maze cues. In a 2 d of pretraining, mice were allowed to familiarize themselves with the maze and eat food pellets for 5 min. For the testing, four arms (one, two, four, seven) were baited with a single food pellet, their position remaining the same from day to day. At the beginning of each trial, a mouse was placed at the center of the maze and allowed to explore it. The trial ended when all food pellets had been eaten, or after 25 entries into the arms of the maze. The trials were repeated twice a day for 14 d. In each trial, the total exploration time was evaluated, and errors were computed: (1) entries in previously visited arms (errors of working or short-term memory) and (2) first entries in unbaited arms (errors of reference or long-term memory). The total number of errors was calculated. The initial and final level of accuracy was estimated by the mean number of errors displayed in the first 3 and last 3 d of the experiment.

The retention and the transfer experiments were started 31 and 32 d after completion of the learning test. The previously unbaited arms were baited (three, five, six, eight), and a new learning test was performed as above.

A two-way repeated-measures ANOVA (treatment × time) was performed to assess differences in the learning curves. *t* test was performed to assess statistical significances of differences in level of accuracy.

Open field test was performed as described (Ammassari-Teule et al., 1994). The mouse was placed on the platform and allowed to explore it for 10 min. The number of lines crossed within this period was counted.

Rotarod test was performed as described (Dunham and Miya, 1957). The time counter started when the mouse was positioned on a rotating cylinder and stopped either when the mouse fell from its cylinder or after 120 sec.

RESULTS

Production of anti-NGF transgenic mice

The rat anti-NGF monoclonal antibody αD11 (Cattaneo et al., 1988) neutralizes the biological action of NGF, *in vitro* (Cattaneo et al., 1988) and *in vivo* (Berardi et al., 1994; Molnar et al., 1997, 1998). The epitope of mAb αD11 on NGF includes the loop region from residues 41–49 (Gonfloni, 1995), which contributes to the interaction surface between NGF and its high-affinity receptor TrkA and distinguishes NGF from other members of the neurotrophin family (Ibanez, 1995, 1998). MAb αD11 does not bind to other neurotrophins and does not block their biological activity (Gonfloni, 1995; Molnar et al., 1998).

The variable regions of the light and heavy chains of mAb αD11 were cloned and reassembled with the human K and γ1 constant regions, respectively (Ruberti et al., 1993), to facilitate the detection of transgenic antibodies against the background of mouse Igs. The heavy and the light chains of the chimeric recombinant antibody were each placed under the transcriptional control of the early region promoter of the human CMV (Boshart et al., 1985) in two separate plasmids (Fig. 1*A*). The linearized DNA was microinjected, either individually or in combination, in fertilized mouse eggs.

Two founder mice with the light chain transgene, two with the heavy chain transgene, and three double-transgenic mice were generated. The serum of double-transgenic mice displayed 50 ng/ml of transgenic anti-NGF antibodies. Despite an intensive breeding program, no offspring were generated.

To overcome this problem and obtain mice expressing a functional antibody constituted by the two chains, mice homozygous for the αD11 heavy chain transgene (VH-αD11 mice, lines C and D) (Fig. 1*B*) were crossed with mice homozygous for the αD11 light chain transgene (VK-αD11 mice, lines A and B) (Fig. 1*B*). Of the two VK-αD11 lines, line A yielded a lower VK genomic signal than line B. For the heavy chain transgenic lines, line C yielded a higher VH genomic signal than line D (Fig. 1*D*). To obtain mice expressing both chains, and thus reconstituting NGF binding activity, single-transgenic mice were intercrossed in different combinations (Table 1). Crossing lines VK-αD11 A with VH-αD11 D and lines VK-αD11 B with VH-αD11 C gave rise to viable pups (family 1 and family 2, respectively) that thrive to adulthood, with a viability >80% (Table 1). On the contrary, the breeding of the two high expression lines VK-αD11 B with VH-αD11 D (family 5) yielded no viable offspring (Table 1).

Expression of transgenic anti-NGF antibody chains

The mRNA levels of the αD11 heavy chain transgenes in tissues of adult mice were much higher in line D than in line C (Fig. 1*D*). For the light chain, lower mRNA expression levels were found in line A (VK low) than in line B (VK high) (data not shown).

As expected for the ubiquitous CMV promoter (Baskar et al., 1996), the VH and VK mRNAs were widely expressed in different adult organs, including brain, kidney, heart, liver, testis (Fig. 1*D*, *E,* and data not shown). For both chains the mRNA levels in adult tissues were much higher than those in neonatal tissues (Fig. 1*E*).

Immunohistochemistry confirmed that both antibody chains could be detected in non-neuronal tissues and in many areas of the brain, including cortex, hippocampus, thalamus, spinal cord, retina, olfactory bulb, and cerebellum (the latter shown in Fig. 2*A*). The association of the heavy and light chains, to reconstitute a functional and secreted antibody, requires that the two chains be coexpressed within the same cell. Double-labeling immunohistochemistry demonstrated the coexpression of the two chains in a high percentage of neuronal and non-neuronal cells (Fig. 2*B*). The number of cells coexpressing both antibody chains was much greater in the adult than in the neonatal tissues (data not shown). At postnatal day 1 (P1), anti-NGF transgenic antibodies were below the detection threshold but could be readily detected in the serum and in the brain (Fig. 2*C*) of P90 adult transgenic mice of family 1 and family 2, reaching levels three orders of magnitude higher than the detection threshold (0.1 ng/ml and 0.1 ng/mg in the serum and in the brain). At P90, the levels of antibodies in serum and brain of family 2 were twofold higher than those in family 1.

When double-transgenic females from family 2 were crossed with VK-αD11 B males to obtain family 3 (Table 1), pups were born alive, but despite evidence of food intake, they did not gain weight and most died within 1 week. The pups that could survive (at most up to 3 weeks) demonstrated a decreased body weight and a delay in hair growth and in the time of eye opening (Fig. 2*D*). Soon after birth, these mice showed tremor of the head, which was more evident during locomotion.

Phenotypic knockout of NGF in the CNS and PNS of adult transgenic mice

For the phenotypic analysis of family 1 and family 2 mice, two groups of controls were used: wild-type mice and the corresponding single-transgenic controls, expressing only the VH-αD11 heavy chain (C or D, as appropriate; see Table 1). Because the heavy chain cannot be secreted in the absence of a cognate light chain and is accumulated intracellularly in the endoplasmic reticulum (Haas and Wabl, 1983), this group of mice also controls for any toxic effects caused by the intracellular accumulation of a foreign protein. Immunohistochemical and Western blot analysis

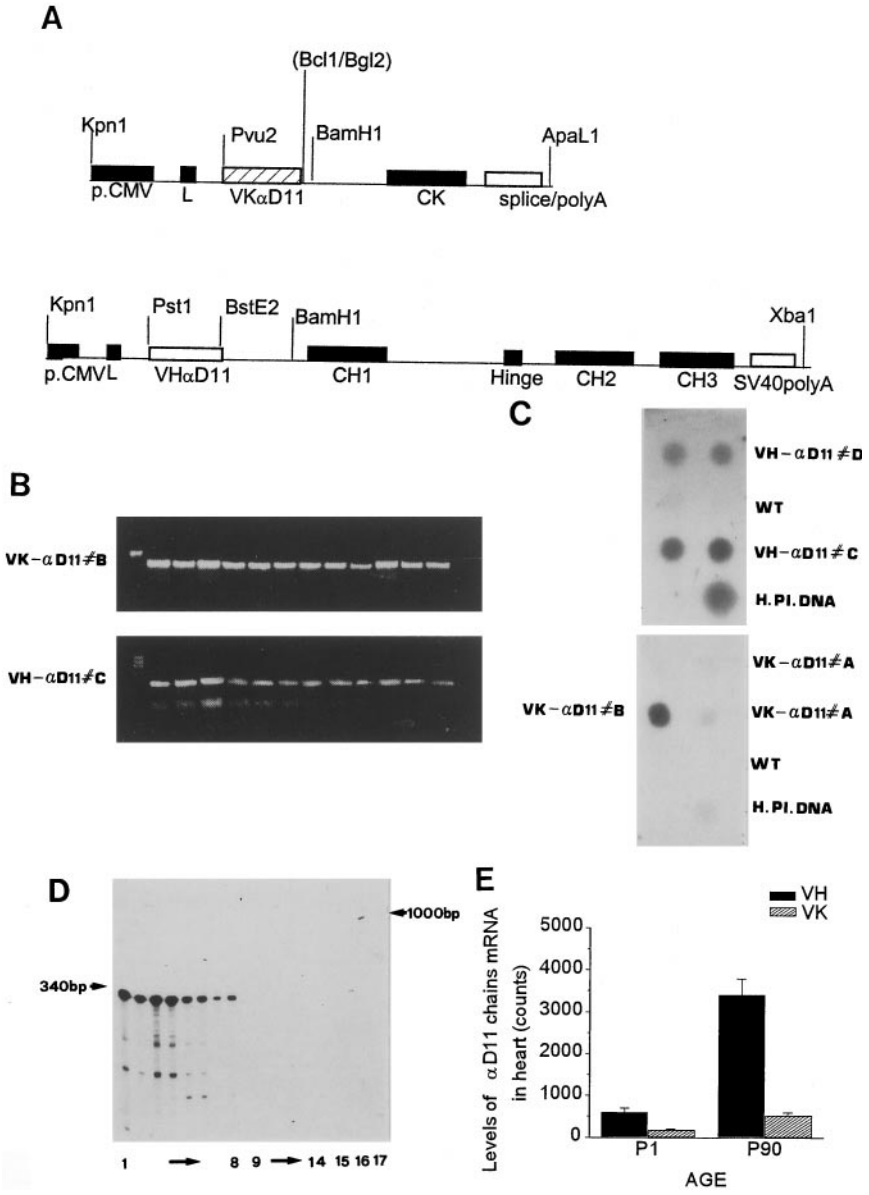

Figure 1. Production of anti-NGF transgenic mice. *A*, DNA constructs for the production of the transgenic mice: light chain (*top panel*) and heavy chain (*bottom panel*) transgenes. *CK* and *CH1–CH3*, Human constant region domains of light (*K*) and heavy (γ1) chains; *VK* and *VH*, light and heavy chain variable regions of the αD11 monoclonal antibody; *CMV*, cytomegalovirus promoter. *B*, PCR analysis to detect the presence of VK (*top panel*) and VH (*bottom panel*) transgenes. The gels show 12 littermates born from homozygous VK (*top panel*) or VH (*bottom panel*) mice crossed to negative mice to verify homozygosis of the single transgenic lines. As evidence, all littermates carry the transgene. *C*, Dot blot analysis of the four lines of mice expressing the heavy or light chain. The *top panel* was probed with a human heavy chain constant region probe and the *bottom panel* with a human light chain constant region probe (see Materials and Methods). DNA samples in the top panel: duplicates of *VH-αD11 #D*, wild-type (*WT*, negative control) and *VH-αD11 #C*, single sample of human placental DNA (*H.Pl.DNA*, positive control). DNA samples in the *bottom panel*: duplicate of *VK-αD11#A*, single samples of *VK-αD11#B*, *WT* (negative control), and human placental DNA (*H.Pl.DNA*, positive control). *D*, Rnase protection analysis of the transgenic VH chain expression in adult kidney and brain of *VH-αD11#D* (*lanes 1-8*) and *VH-αD11#C* (*lanes 9-14*) mice. *Lane 15*, RNA from wild-type mouse brains. *Lane 16*, RNA from a cell expressing the recombinant mAb αD11. *Lane 17*, VH RNA probe. *E*, Levels of VH-αD11 and VK-αD11 mRNA in heart at P1 and P90 of mice from family 1, evaluated by phosphorimaging analysis, normalized to the β-actin mRNA (mean counts ± SEM). Number of mice for each age, $n = 6$.

showed that the heavy chain levels in the single-transgenic lines are identical to those in the corresponding double-transgenic lines (data not shown). In all of the phenotypic analyses performed, wild-type mice and transgenic controls were indistinguishable.

During the first 3–4 postnatal weeks, family 1 and family 2 mice showed no macroscopically visible abnormalities except a small decrease in body weight (25% less than that of control mice).

In the CNS, the histological analysis revealed that the number of ChAT-positive neurons was decreased in the BF (Fig. 3*A,B*) and the hippocampus (Fig. 3*I,L*).

The stereological analysis revealed that the volume of the BF of anti-NGF transgenic mice was equal to $3.8 \times 10^9 \pm 4.2 \times 10^8$ μm^3, and it was not different from that calculated for transgenic controls ($4.2 \times 10^9 \pm 4.0 \times 10^8$ μm^3). In particular, the volume of the medial septal nucleus is not changed, being $2.1 \times 10^9 \pm 1.6 \times 10^8$ μm^3 in anti-NGF mice and $2.2 \times 10^9 \pm 1.5 \times 10^8$ μm^3 in transgenic controls. The number of ChAT-positive neurons in the BF and the hippocampus of neonatal and P10 transgenic mice was not affected (Table 2). In adult transgenic mice, the number of ChAT-positive neurons was evaluated by two different methods: the stereological estimation of the total number of cells and the mean number of ChAT-positive cells per millimeters squared (Table 2). Both methods showed that in adult transgenic mice the number of ChAT-positive neurons was much lower than in controls. The stereological analysis revealed that the total number of ChAT-positive neurons in the BF of anti-NGF mice was 6327 ± 621, whereas in transgenic controls it was 8726 ± 375 ($p < 0.05$). In particular, the calculated values for the medial septum revealed a decrease equal to the 42.8% (3153 ± 201 ChAT-positive neurons in anti-NGF mice vs 5475 ± 235 neurons in control mice, $p < 0.05$). The values calculated using the mean number of ChAT-positive cells are reported in Table 2, for both the basal forebrain and the hippocampus.

ChAT-positive fibers projecting to the cortex and the hippocampus of transgenic mice were more lightly stained than in control mice (Fig. 3*C,D*). The remaining ChAT-positive neurons were less intensely stained (data not shown), and their cell bodies showed a marked shrinkage. This can be observed in the high-magnification field shown in Figure 3*F,H*, in which BF cells from anti-NGF transgenic mice are labeled with anti-TrkA and anti-

Table 1. Scheme of the different crossings between mice expressing the light chain with mice expressing the heavy chain

Crossings	Offspring	Viability
F (VK low) × M (VH high) Line A Line D	VK low/VH high (family 1)	Adult (>80%)
F (VK high) × M (VH low) Line B Line C	VK high/VH low (family 2)	Adult (>80%)
F (VK high/VH low) × M (VK high) Family 2 Line B	VK high (homozygous)/VH low (family 3)	<P20 (100%)
F (VK high/VH low) × M (VK low) Family 2 Line A	VK high-VK low/VH low (family 4)	Adult (50%)
F (VK high) × M (VH high) Line B Line C	VK high/VH high (family 5)	<P1 (100%)
F (VK high/VH low) × M (wild type) Family 2 WT	VK high/VH low (family 6)	Adult (>80%)

p75 antibodies, respectively. These figures also show a marked decrease in the number of TrkA (Fig. 3*E*,*F*) and p75 (Fig. 3*G*,*H*) immunoreactive cells. No evidence was found for apoptotic cell death in the BF region of transgenic mice, as assessed by the TUNEL method for DNA fragmentation (data not shown).

In the hippocampus, the extent of CA3 mossy fibers was evaluated in anti-NGF mice by the Timm's procedure, revealing a marked reduction in the zinc staining with respect to controls (Fig. 3*M*,*N*).

In the PNS, SCG from 2-month-old anti-NGF transgenic mice were markedly smaller than those from transgenic controls, as shown in corresponding transverse sections (Fig. 4*A*,*B*). The area of the middle section from the transgenic SCG was 45% of that from control mice. No pyknotic nuclei were observed in SCG from anti-NGF transgenic mice, but the size of the cells was greatly reduced, with respect to control mice (Fig. 4*C*,*D*). The extent of cell body shrinkage is shown in Figure 4*S* and corresponds to a variation of the median value of the distribution from 225 to 175 μm^2. The minimum and maximum values of the median for individual mice in each group were 218.4 and 311.76 μm^2 for control mice and 156.99 and 193.28 μm^2 for transgenic anti-NGF mice.

The size of neurons of lumbar DRG from transgenic mice was dramatically reduced, and the majority of neurons displayed clearly pyknotic nuclei (Fig. 4*E*,*F*). The reduction of the cell body size is demonstrated in Figure 4*T* and corresponds to a variation of the median value of the distribution from 425 to 75 μm^2. The minimum and maximum values of the median for individual mice in each group were 515.32 and 755.47 μm^2 for control mice and 61.15 and 91.86 μm^2 for transgenic anti-NGF mice.

The phenotypic analysis of DRG neurons revealed that the number of TrkA- (Fig. 4*G*,*H*) and p75-positive neurons (Fig. 4*I*,*L*), but not that of TrkB-positive neurons (Fig. 4*M*,*N*), was markedly reduced in DRG from transgenic mice. Also the number of CGRP- (Fig. 4*O*,*P*) and SP-positive neurons (Fig. 4*Q*,*R*) was reduced in transgenic mice. In the latter case, the spared SP-positive neurons were more lightly stained in transgenic than in control mice. This observation correlates well with the reduced number of SP-immunopositive fibers observed in the skin of

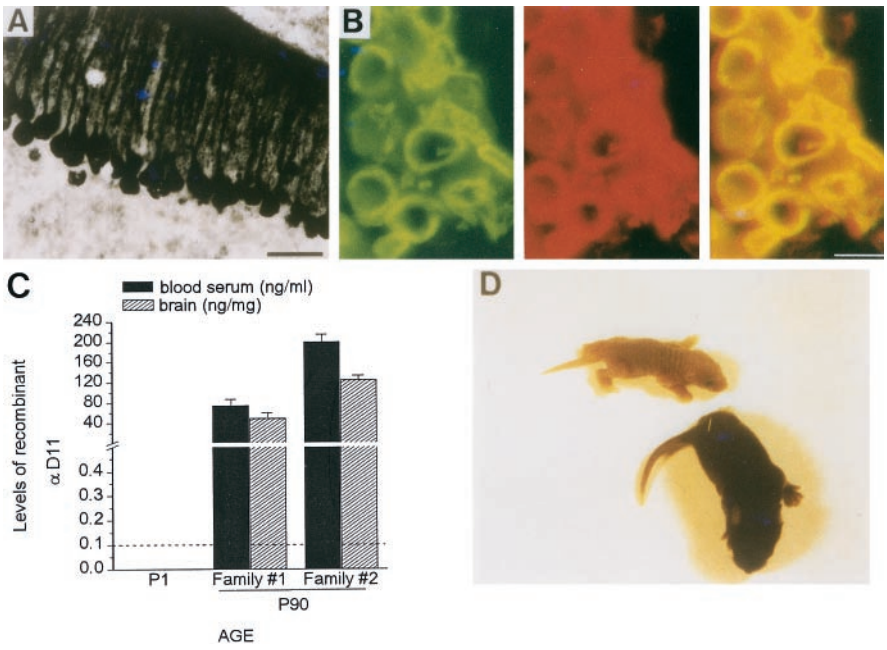

Figure 2. Expression of functional antibodies in anti-NGF transgenic mice. *A*, Expression of the recombinant VH in Purkinje cells of the cerebellum of VH-αD11 C mice. Scale bar, 38 μm. *B*, Expression of VH (*green*) and VK (*red*) chains, in DRG of family 1 mice. The coexpression of the two chains in the same cells is shown in the *right panel* (*yellow*). Scale bar, 25 μm. *C*, Level of recombinant αD11 in the serum and in the brain of *Family #1* and *Family #2* mice, at *P1* and *P90* (values are mean ± SEM, $n = 6$ for each group). The *horizontal dotted line* represents the detection threshold of the assay (0.1 ng/ml). *D*, A transgenic control (transgenic for VH only) and a transgenic anti-NGF (family 3) mouse at P17. The transgenic mouse is much smaller than the control.

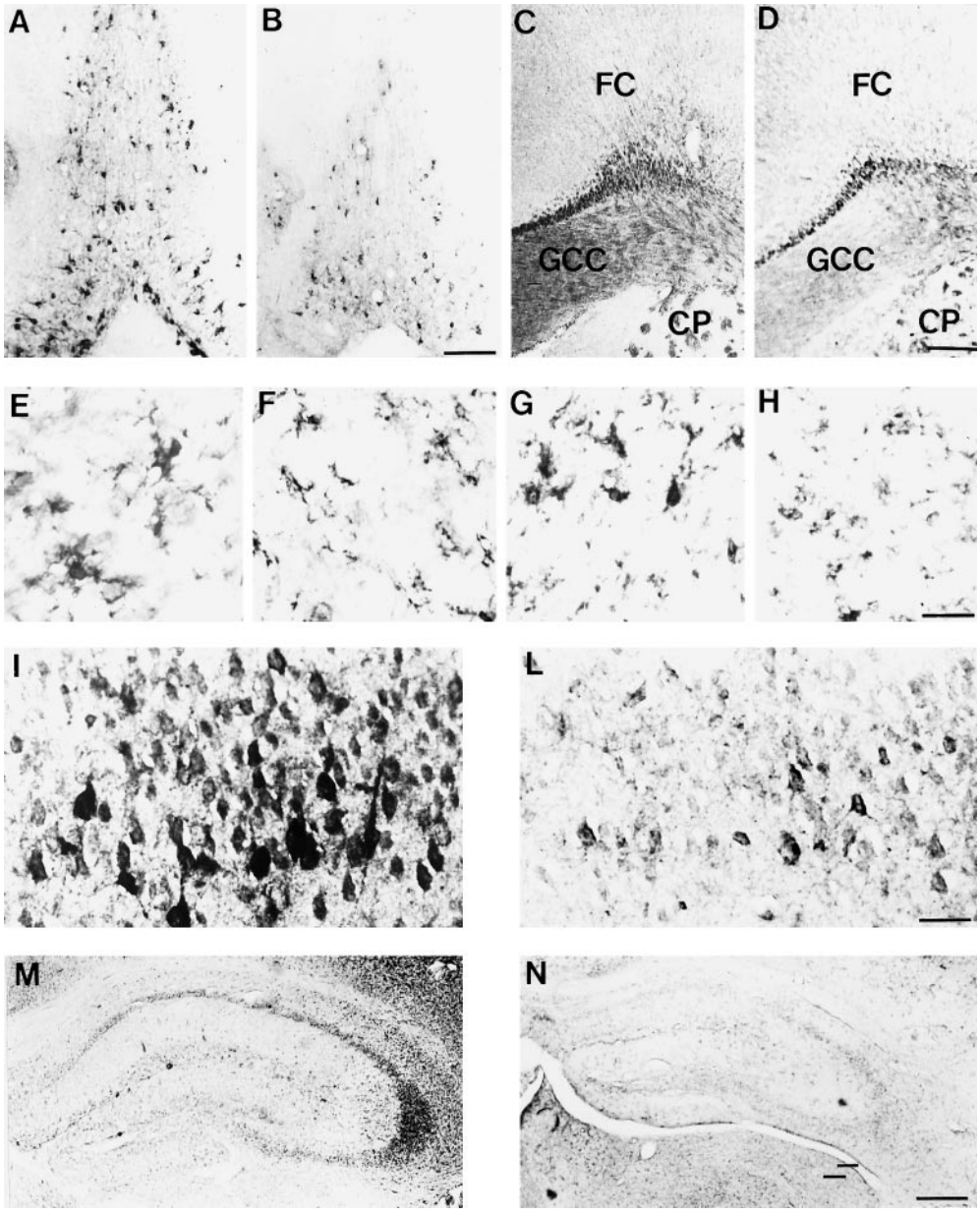

Figure 3. Phenotypic analysis of the CNS of anti-NGF transgenic mice. *A–H*, Sections through the BF: ChAT-positive neurons in control (*A*) and anti-NGF transgenic mice (*B*). Cholinergic innervation to the frontal cortex, stained with anti-ChAT, in control (*C*) and anti-NGF transgenic mice (*D*). *CP*, Caudate/putamen; *FC*, frontal cortex; *GCC*, genu corpus callosum. TrkA-positive neurons of the BF in control (*E*) and anti-NGF transgenic mice (*F*). p75-positive neurons in the BF of control (*G*) and anti-NGF transgenic mice (*H*). ChAT staining of hippocampal section in control (*I*) and anti-NGF transgenic mice (*L*). Timm's staining in hippocampal mossy fibers of control (*M*) and anti-NGF transgenic mice (*N*). Scale bars: *A–D*, *M–N*, 300 μm; *E–H*, 150 μm; *I–L*, 38 μm. The figures are representative of an analysis performed on 10 animals for each group.

anti-NGF mice compared with transgenic controls (data not shown).

Immunohistochemical analysis of trigeminal, nodose, petrose, and vestibular ganglia of transgenic mice, with antibodies against TrkB, TrkC, BDNF, and NT-3, as appropriate, did not reveal any difference with respect to the corresponding ganglia of control mice (data not shown). This shows that neurons sensitive to other neurotrophins are not affected, as expected, given the specificity of the αD11 antibody.

Skeletal muscles of transgenic mice show a marked dystrophy

Adult transgenic mice of families 1 and 2 often showed a waddling gait (Fig. 5*A*), attributable to an abnormal position of the hind limbs, that was also demonstrated when the mice were held by their tail (Fig. 5*C*,*D*). Moreover, these mice walked on the tiptoes of their hind feet. Very often these mice developed a scoliosis of the back (Fig. 5*B*).

Anatomical analysis of skeletal muscles from adult anti-NGF transgenic mice revealed a macroscopic reduction of the mass of longitudinal dorsal muscles and the flexor and abducent muscles of the hind limbs. This atrophy was not observed in other muscles, such as those forming the abdominal wall and the flexor and abducent muscles of the fore limbs.

Muscle fibers of the dorsal muscles of anti-NGF mice showed a markedly decreased cross-sectional area and a more irregular shape (Fig. 5*E*,*F*). Quantification of the cross-sectional area of single fibers revealed a very significant reduction of large cross-section cells (Fig. 5*G*). The difference in the color of myofibers stained with hematoxylin/eosin most likely reflects the presence of sarcoplasmic deposits. The amyloid nature of these deposits was suggested by a positive staining of transgenic myofibers with Congo red (data not shown), which formed a ring-shaped region beneath the sarcolemma.

The dystrophy of skeletal muscles was not observed in young animals (between P2 and P30), when the antibody levels are undetectable (P2) or start to increase (P30).

Table 2. Number of ChAT-positive cells in the basal forebrain and hippocampus of transgenic controls and anti-NGF transgenic mice

	Mice	Age	ChAT-positive neurons (cells/mm^2)	Minimum value (cells/mm^2)	Maximum value (cells/mm^2)	% Reduction
BF	VH	Adult	113.28 ± 3.97	107.25 ± 5.58	120.00 ± 4.94	
	Family 1	Adult	50.91 ± 4.76*	42.25 ± 3.86	56.00 ± 3.36	55
BF	VH	P10	111.37 ± 5.05	105.75 ± 8.55	118.00 ± 2.23	
	Family 1	P10	103.06 ± 3.98	97.25 ± 10.70	108.50 ± 7.53	
Hippocampus	VH	Adult	164.54 ± 10.54	149.00 ± 2.23	176.50 ± 2.29	
	Family 1	Adult	62.50 ± 6.25*	54.50 ± 2.5	71.00 ± 4.84	62
Hippocampus	VH	P10	36.70 ± 3.43	33.66 ± 2.86	42.00 ± 2.94	
	Family 1	P10	35.91 ± 4.22	30.33 ± 1.69	40.33 ± 1.70	

Values are the mean ± SEM (adult mice, $n = 6$; P10, $n = 4$). *$p < 0.01$. The sterological values for the volume and number of ChAT-positive neurons in the BF of anti-NGF and transgenic controls are reported in Results.

Apoptosis in the spleen of anti-NGF transgenic mice

In the spleen of anti-NGF mice, the two antibody chains were expressed in the red pulp (Fig. 6*A*,*B*). In control mice the sympathetic innervation of the spleen was localized around the central artery, and few nerve fibers were seen in the marginal zone (Fig. 6*C*). In transgenic mice the innervating fibers were scattered throughout the germinal center and the marginal zone, without reaching the vessel (Fig. 6*D*).

The total number of viable splenocytes recovered from the spleen of transgenic mice was dramatically lower than that recovered from control mice (2–3 × 10^7 vs 2–3 × 10^6). In transgenic mice the proportion of the spared splenocytes expressing surface IgM and IgA, determined by flow cytometry, was unaffected, whereas the proportion of IgG-positive cells was reduced (Fig. 6*E*) and that of IgD-positive cells showed a small but significant increase (Fig. 6*E*). A similar reduction of the percentage of IgG-positive cells was also demonstrated by immunohistochemistry in spleen sections from transgenic mice (Fig. 6*F*).

The very low recovery of viable splenocytes was suggestive of cell death. The red pulp region in the spleen of anti-NGF trans-

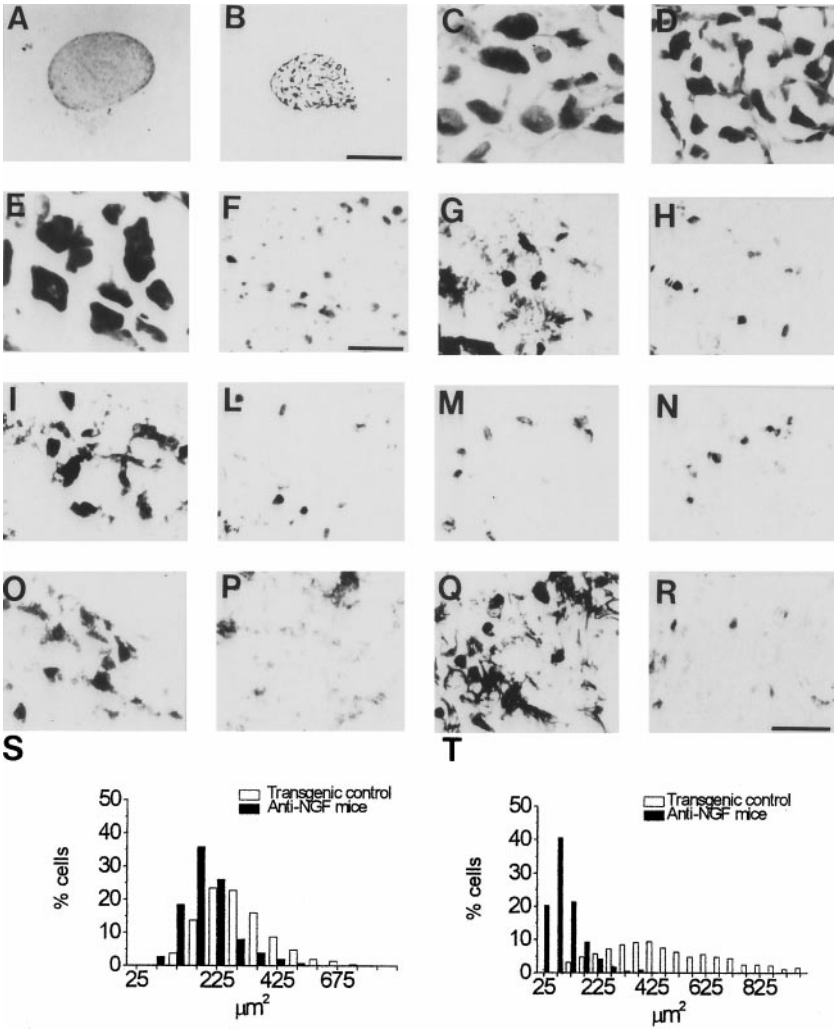

Figure 4. Phenotypic analysis of the PNS of anti-NGF transgenic mice. Cresyl violet staining of SCG (*A–D*) and DRG (*E*, *F*) from control (*A*, *C*, *E*) and anti-NGF transgenic mice (*B*, *D*, *F*) reveals a dramatic decrease in the area of SCG and in cell size of SCG (*S*) and DRG (*T*) with respect to control mice ($n = 6$ for each group of mice). In DRG, immunohistochemistry against TrkA (*G*, *H*), p75 (*I*, *L*), CGRP (*O*, *P*), and SP (*Q*, *R*) shows a decreased intensity of labeling in anti-NGF transgenic mice (*H*, *L*, *P*, *R*) with respect to controls (*G*, *I*, *O*, *Q*). Immunoreactivity against TrkB is unaffected in anti-NGF mice (*N*) versus controls (*M*). Scale bars: *A*, *B*, 1.6 mm; *C–F*, 750 µm; *G–R*, 500 µm.

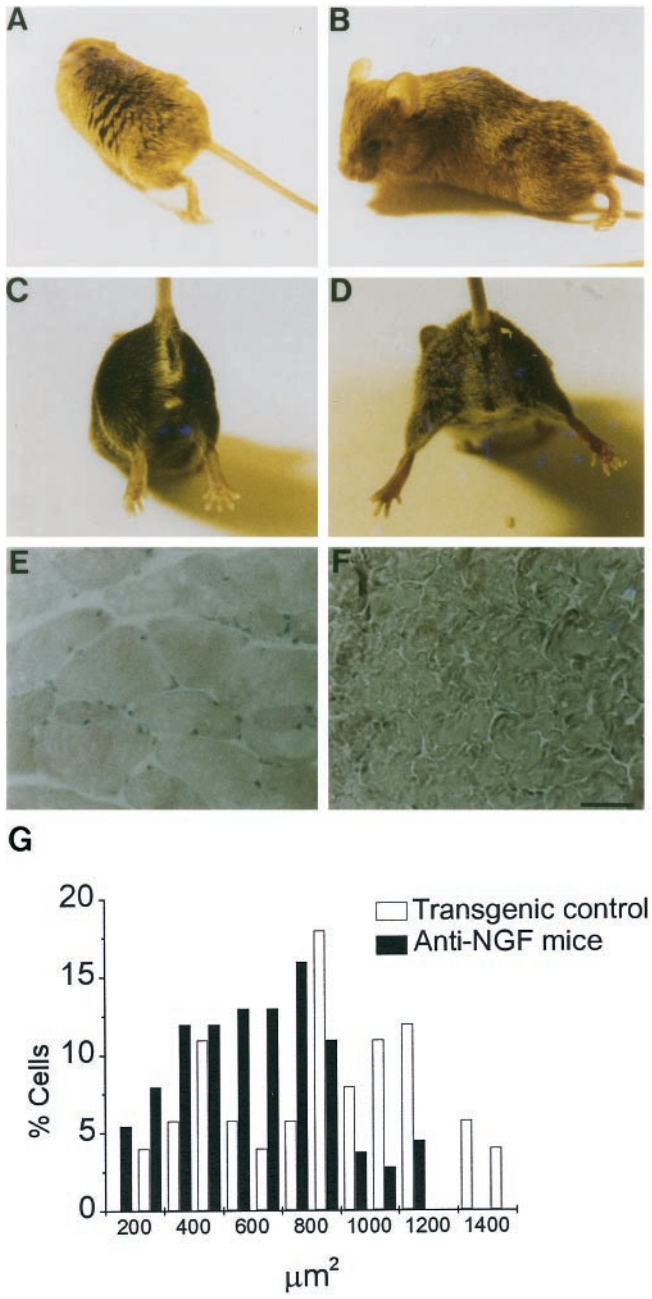

Figure 5. Muscular dystrophy in anti-NGF transgenic mice. Anti-NGF transgenic mice show an abnormal waddling gait (*A*), a marked scoliosis (*B*), and a typical posture of the hind limbs (*D*) versus controls (*C*). Transverse sections through the longitudinal muscle of the back, stained with hematoxylin/eosin of control (*E*) and anti-NGF transgenic mice (*F*), showing a marked decrease in the size of myofibers (*G*). The analysis was performed on six transgenic controls and six anti-NGF transgenic mice. Scale bar (shown in *E* for *E*, *F*): 500 μm.

genic mice contained a large number of apoptotic cells, as evaluated by the presence of DNA fragmentation (Fig. 6*H*). Control spleens (Fig. 6*G*) contained a threefold smaller number of lower intensity labeled cells (Fig. 6*F*). The number of apoptotic cells was greater than that of the cells expressing the transgenic heavy or light chains (Fig. 6*F*), demonstrating that the apoptotic process also occurred in cells not expressing the transgenic antibody chains.

The spleen of young animals (between P2 and P30) showed no sign of apoptosis, even when transgenic antibody chains can be detected at the cellular level.

Behavioral analysis of anti-NGF mice

Behavioral tests were performed in adult transgenic mice from family 1, and care was taken to select litters that did not show a visible abnormality in their walking pattern, such as the one described in Figure 5.

The sensitivity to thermal pain was evaluated in control and transgenic mice by the hot plate test and showed a significant increase in the latency time for licking of the hind paws and jumping (Fig. 7*A*).

The general motor activity of transgenic mice did not differ from that of control mice in the open field test (Fig. 7*B*). A rotarod test was performed (Fig. 7*C*) to assess motor coordination and fatigability, demonstrating a marked impairment in anti-NGF mice.

For spatial learning, mice were tested in a radial maze. The two overall learning curves differed (two-way RMANOVA, $p < 0.05$) (Fig. 7*D*). During the first 3 d, the transgenic mice made a significantly higher number of entries (Fig. 7*D*) and in particular of re-entries in already visited arms (i.e., working memory errors; data not shown). The final level of accuracy in the last 3 d was not significantly different for anti-NGF and control mice. To analyze the ability of mice to retain the performance acquired, mice were tested in the maze 31 d after completion of the learning test, with the same combination of arms baited as during learning. It was evident (Fig. 7*E*) that transgenic mice made as many entries as when first confronted with the task (no statistical difference with the number and type of errors made in the first 3 d). They did not retain the level acquired with learning (significant difference with the final level of accuracy in the last 3 d, paired *t* test, $p < 0.05$), whereas control mice retained the level acquired with learning (Fig. 7*E*).

To test the ability of the mice to transfer their learning capacity to a new situation, the day after the retention test the previously unbaited arms were baited, and a new learning test was performed. The results showed a clear transfer deficit for the transgenic mice (two-way RMANOVA, $p < 0.01$); they still performed significantly worse than control mice after 5 d of training (Fig. 7*F*). The difference in performance was attributable to a significantly higher number of working memory errors (*t* test, $p < 0.006$).

At the completion of the behavioral tests, the phenotype of all mice was analyzed at the histological and immunochemical level, confirming the presence of the neuronal and non-neuronal deficits described.

DISCUSSION

The role of NGF during development of the nervous system has been characterized (Levi-Montalcini, 1987) and more recently, by the disruption of the NGF, p75, and TrkA genes (Lee et al., 1992; Crowley et al., 1994; Smeyne et al., 1994). A role for NGF in adult and aged animals has been suggested. However, because of the lethality of *ngf*−/− mice in the early postnatal period (Crowley et al., 1994), no comprehensive transgenic model in which the actions of NGF in the adult are antagonized or ablated is available.

We used the neuroantibody approach (Piccioli et al., 1991, 1995), based on the local secretion of recombinant antibodies in transgenic mice, to neutralize the activity of NGF. The two-tier

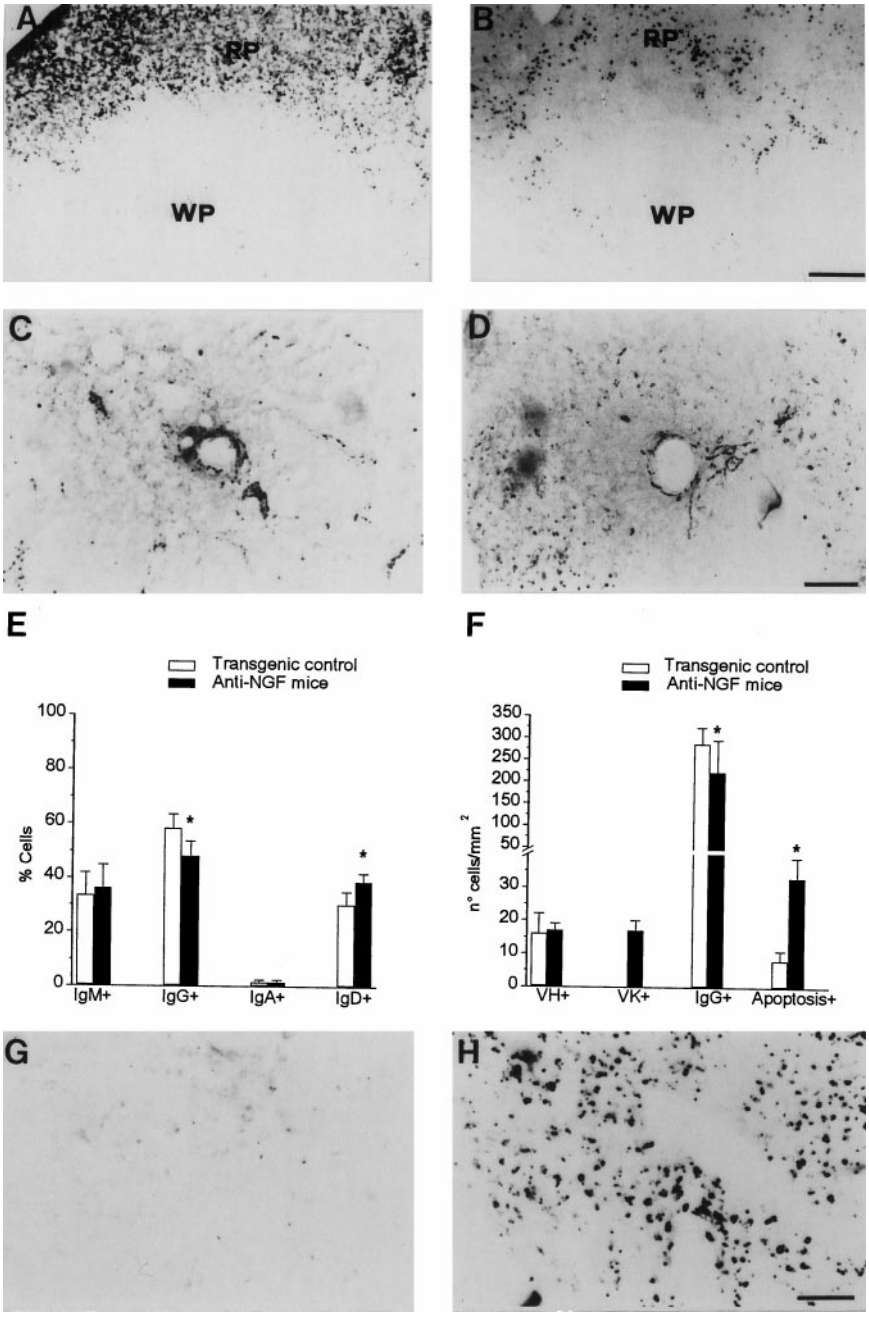

Figure 6. Apoptosis in the spleen of anti-NGF transgenic mice. VH (*A*) and VK (*B*) expression in the spleen of anti-NGF transgenic mice is localized in the red pulp (*RP*) and absent in the white pulp (*WP*). TH immunoreactivity in control mice is localized around the central artery of the WP (*C*), whereas in anti-NGF mice it is localized at the WP periphery (*D*). *E*, Surface phenotype of splenocytes. The flow cytometric analysis was performed on six control mice and six anti-NGF transgenic mice. $^{*}p < 0.05$. *F*, Quantification of the number of splenocytes expressing VH, VK, or IgG or displaying DNA fragmentation. Values are the mean ± SEM, $n = 6$ for family 1 and $n = 6$ for transgenic controls. $^{*}p < 0.05$. *G*, *H*, TUNEL staining of spleen sections from control (*G*) and transgenic (*H*) mice. Scale bars: *A–D*, 300 μm; *G*, *H*, 1000 μm.

approach, in which separate transgenic lines expressing individual chains are crossed, allowed us to limit the developmental consequences deriving from exposure of fetuses and newborns to anti-NGF antibodies (Gorin and Johnson, 1980; Johnson et al., 1980). By exploiting different breeding combinations (Table 1), it was possible to modulate the severity of the phenotypic knockout. The lethal phenotype observed with some of the transgenic combinations (families 3 and 5; Table 1) validates the model's ability to achieve a phenotypic neutralization of NGF as complete as in *ngf*−/− mice (Crowley et al., 1994). The lethal outcome is not determined by maternally derived antibodies, because pups born from the same double-transgenic females, crossed to a negative male, are viable (family 6). Thus, the additional expression of the VK transgene in the embryos appears to determine the lethal phenotype. Newborns of family 4 show a 50% viability (Table 1). On the other hand, mice from families 1 and 2 reach adulthood, when the antibody levels are more than 1000-fold higher than at birth. The limited increase (sixfold) in total mRNA levels for the individual chains during the postnatal period corresponds to an increase in the number of cells expressing each transgene, leading to a dramatic increase in the number of cells coexpressing both transgenes.

The phenotypic analysis of independent families showed consistent results, ruling out chromosomal integration-dependent effects. The phenotypes observed across litters of the same genotype were fully penetrant. The only limited variability observed relates to the abnormalities in the walking pattern (see Results), which can vary in the age of onset but eventually are present in all transgenic mice older than 6 months.

Anti-NGF antibodies in the serum and the brain are sufficiently

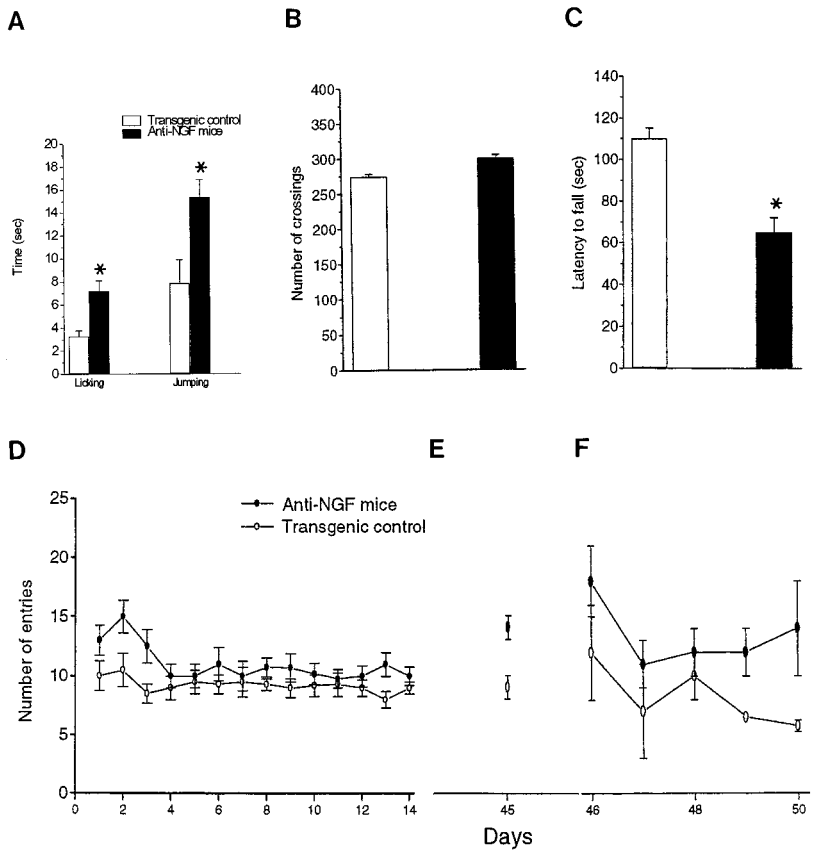

Figure 7. Behavioral analysis of anti-NGF transgenic mice. *A*, Nociceptive test in anti-NGF transgenic and transgenic control mice. Values are the mean ± SEM, $n = 10$ for each group of animals. *B*, Open field test. *C*, Rotarod test. $^*p < 0.05$. *D*, Spatial learning curves for anti-NGF transgenic ($n = 10$, ●) and control ($n = 10$, ○) mice in a radial eight-arm maze (4 arms baited). Vertical bars are the SEs. The number of arm entries necessary to find all four food pellets is reported as a function of time. *E*, Retention test, 31 d after the end of the learning test. *F*, Transfer test, started the day after the retention test.

Table 3. Amount of free NGF and transgenic antibody in different tissues from transgenic control and anti-NGF transgenic mice

Tissue	Mice	Free NGF	% Reduction[a]	αD11 recombinant antibody
Submaxillary gland	VH	2.77 ± 0.17 μg/mg		
	Family 1	1.92 ± 1.92 μg/mg*	30.6	82.9 ± 9.42 ng/mg
Brain	VH	31.3 ± 1.88 ng/mg		
	Family 1	16.6 ± 1.33 ng/mg*	53	57.3 ± 10.37 ng/mg
Dorsal muscles	VH	11.6 ± 1.24 ng/mg		
	Family 1	4.5 ± 1.70 ng/mg*	61.2	50.6 ± 1.24 ng/mg
Abdominal muscles	VH	10.3 ± 2.62 ng/mg		
	Family 1	11.3 ± 1.24 ng/mg	10.3	12.6 ± 2.05 ng/mg
Blood	VH	46.3 ± 2.62 pg/ml		
	Family 1	22.3 ± 2.35 pg/ml*	48.1	116 ± 18.45 ng/ml

Values are the mean ± SEM ($n = 3$). $^*p < 0.001$.

[a]% reduction of free NGF in anti-NGF transgenic mice with respect to transgenic controls.

abundant to neutralize NGF biological activity but are well below the range of concentrations at which the cross-reactivity with other neurotrophins was tested and ruled out (Gonfloni, 1995; Molnar et al., 1998). Adverse effects arising from immune complexes involving transgenic anti-NGF antibodies could be excluded, because no antibody accumulation was detected in the kidneys (data not shown).

The phenotype of adult mice revealed complex and severe deficits. Interestingly, heterozygous *ngf*+/− mice do not exhibit gross morphological abnormalities and contain ~75% of the NGF levels in control mice (Chen et al., 1997). The levels of residual free NGF, not bound to the transgenic antibodies, in adult anti-NGF transgenic mice are ~50% of the circulating NGF levels in control mice (Table 3). It should be noted that the assay used for this determination overestimates the amount of free NGF, because NGF dissociates from the antibodies during the extraction process. Moreover, the time course of NGF neutralization in heterozygous *ngf*+/− and in anti-NGF transgenic mice is very different. Thus, the neuroantibody approach leads to an effective neutralization of NGF activity in adult mice, attributable to the antibody preventing the binding of NGF to TrkA and p75 receptors (Gonfloni, 1995). Because the antibody does not recognize receptor-bound NGF, complement-mediated cell killing can be excluded.

The analysis of adult mice showed deficits in well known NGF targets, such as SCG (Levi-Montalcini and Angeletti, 1966) and DRG (Ruit et al., 1992; Silos-Santiago et al., 1995).

In the CNS of transgenic mice, we have studied cholinergic neurons in the BF region (Korsching, 1986) and the hippocampus (Vijayan, 1979). The role of NGF in modulating the survival and phenotype of adult cholinergic neurons is controversial (Rylett and Williams, 1994; Snider, 1994). Here we demonstrate that adult anti-NGF mice show a stable decrease of ChAT expression in the BF and hippocampal cholinergic neurons, in addition to marked cell shrinkage. A critical period in the sensitivity of BFCNs to NGF deprivation has been suggested (Molnar et al., 1997; 1998), on the basis of a significant but transient and reversible cholinergic deficit. This suggested a "negative priming" model (Molnar et al., 1998), whereby a complete disruption of NGF activity during development (Crowley et al., 1994; Molnar et al., 1998) would lead, after a transient downregulation, to the independence of BFCNs from NGF. In the presence of an incomplete block of NGF, such as in *ngf*+/− mice, BFCNs would maintain their dependence from NGF throughout life, as observed by Chen et al. (1997). The cholinergic deficit observed in BFCNs of adult anti-NGF transgenic mice is more severe than in *ngf*+/− mice and confirms the negative priming hypothesis. These results establish that in adult mice the cholinergic function of BFCNs can be severely impaired by NGF deprivation, provided that NGF is not limiting during the early postnatal period. Notwithstanding the severe cholinergic deficit, no cell death was observed.

The decrease in the Timm's staining of mossy fibers in the CA3 area of the hippocampus of anti-NGF mice parallels the efficacy of αD11 to affect synaptic plasticity in CA3 during development (Ruberti et al., 1997) and supports a role of NGF in the remodeling of neuronal circuitries in adult animals (Rashid et al., 1995; Van der Zee et al., 1995; Debeir et al., 1999).

A functional correlate of the anatomical cholinergic deficits was established by showing a significant impairment in spatial learning tasks in anti-NGF mice that was particularly evident in retention and transfer tasks. Noteworthy is the strong deficit for working memory, which correlates with the effectiveness of NGF treatment in ameliorating working memory in aged rats, possibly through the BF cholinergic system (Markowska et al., 1996; Frick et al., 1997; Gustilo et al., 1999). The increased threshold of the anti-NGF mice for noxious stimuli confirms the activities of the NGF/TrkA system in the modulation of chronic pain (Levine, 1998; Snider and McMahon, 1998) and proposes these mice as a model for nociception. Anti-NGF mice showed impairment in the rotarod test that could be ascribed to their muscular atrophy. However, because the rotarod test assesses multiple systems, we cannot exclude the involvement of single or multiple combinations of distinct neuronal NGF-responsive populations.

Adult anti-NGF mice were used to study non-neuronal sites of NGF actions, such as spleen and skeletal muscles.

In the spleen, neutralization of NGF leads to an incomplete maturation of its sympathetic innervation (Carlson et al., 1995), which is known to correlate with NGF levels in target tissues (Korsching and Thoenen, 1983; Shelton and Reichardt, 1984).

Actions of NGF on T- and B-lymphocytes have been postulated (Cattaneo 1985; Ehrhard et al., 1993a,b), but evidence of a modulatory role on the B-cell-dependent immune response has been presented only recently (Torcia et al., 1996). To our knowledge, the immune system in *ngf*+/− heterozygous mice has not been studied. Anti-NGF mice show a dramatic loss of viable splenocytes, reflecting a process of cell death by apoptosis. Control spleens show a background of cells weakly labeled for DNA fragmentation that might be related to chromosomal rearrangements of immunoglobulin loci or to a physiological process of cell death. The expression of rearranged secretory transgenic antibody chains in lymphocytes is not causing cell death. Indeed, the number of cells with DNA fragmentation is higher than that of cells expressing either chain. Transgenic mice expressing rearranged antibody genes in B-lymphocytes have been produced before (Storb et al., 1986; Neuberger et al., 1989; Pettersson et al., 1989), without signs of lymphocyte death.

Anti-NGF mice revealed an unexpected dystrophy affecting spinal and hindlimb extensor muscles but not abdominal and hindlimb flexor muscles. The differential effect between muscles could reflect different antibody levels (Table 3) or intrinsic differences between muscles. Muscular dystrophy was not described in NGF or TrkA knockout mice (Crowley et al., 1994; Smeyne et al., 1994), most likely because of their premature death. The muscular dystrophy could result from a direct action of NGF on developing or adult myofibers expressing NGF receptors (Baron et al., 1994; Yamamoto et al., 1996; Seidl et al., 1998) or from an indirect effect involving a cascade of NGF-induced changes in gene expression, leading to an altered phenotype of spinal motoneurons expressing the p75 receptor (Sendtner et al., 1996). However, this hypothesis cannot be easily reconciled with the lack of a muscular phenotype in p75 knockouts (Lee et al., 1992) and with the absence of gross cellular abnormalities in the ventral horn of the spinal cord of anti-NGF mice.

This transgenic model lends itself to a future characterization of the consequences of NGF deprivation in aged mice.

REFERENCES

Ammassari-Teule M, Fagioli S, Rossi-Arnaud C (1994) Radial maze performance and open-field behaviours in aged C57BL/6 mice: further evidence for preserved cognitive abilities during senescence. Physiol Behav 55:341–345.

Baron P, Scarpini E, Meola G, Santilli I, Conti G, Pleasure D, Scarlato G (1994) Expression of the low-affinity NGF receptor during human muscle development, regeneration, and in tissue culture. Muscle Nerve 17:276–284.

Baskar JF, Smith PP, Nilaver G, Jupp RA, Hoffmann S, Peffer NJ, Tenney DJ, Colberg-Poley AM, Ghazal P, Nelson JA (1996) The enhancer domain of the human cytomegalovirus major immediate-early promoter determines cell type-specific expression in transgenic mice. J Virol 70:3207–3214.

Berardi N, Cellerino A, Domenici L, Fagiolini M, Pizzorusso T, Cattaneo A, Maffei L (1994) Monoclonal antibodies to nerve growth factor affect the postnatal development of the visual system. Proc Natl Acad Sci USA 91:684–688.

Boshart M, Weber F, Jahn G, Dorsch-Asler K, Fleckenstein B, Schaffner W (1985) A very strong enhancer is located upstream of an immediate early gene of human cytomegalovirus. Cell 41:521–530.

Carlson SL, Albers KM, Beiting DJ, Parish M, Conner JM, Davis BM (1995) NGF modulates sympathetic innervation of lymphoid tissues. J Neurosci 15:5892–5899.

Cattaneo A (1985) Thymocytes as potential target cells for nerve growth factor. In: Molecular aspects of neurobiology (Levi Montalcini R, Calissano P, Kandel ER, Maggi A, eds), pp 31–36. New York: Springer.

Cattaneo A, Neuberger MS (1987) Polymeric immunoglobulin M is secreted by transfectants of non-lymphoid cells in the absence of immunoglobulin J chain. EMBO J 6:2753–2758.

Cattaneo A, Rapposelli B, Calissano P (1988) Three distinct types of monoclonal antibodies after long term immunization of rats with mouse NGF. J Neurochem 50:1003–1010.

Chen KS, Nishimura MC, Armanini MP, Crowley C, Spencer SD, Phillips

HS (1997) Disruption of a single allele of the nerve growth factor gene results in atrophy of basal forebrain cholinergic neurons and memory deficits. J Neurosci 17:7288–7296.
Chomcynzski P, Sacchi N (1987) Single-step method of RNA isolation by acid guanidinium thiocyanate-phenol-chloroform extraction. Anal Biochem 162:156–159.
Crowley C, Spencer SD, Nishimura MC, Chen KS, Pitts-Meek S, Armanini MP, Lanway HL, McMahon SB, Shelton DL, Levinson AD, Phillips HS (1994) Mice lacking nerve growth factor display perinatal loss of sensory and sympathetic neurons yet develop basal forebrain cholinergic neurons. Cell 76:1001–1011.
Cuello C, Galfré G, Milstein C (1979) Detection of substance P in the central nervous system by a monoclonal antibody. Proc Natl Acad Sci USA 7:3532–3536.
Debeir T, Saragovi HU, Cuello C (1999) A nerve growth factor mimetic TrkA antagonist causes withdrawal of cortical cholinergic boutons in the adult rat. Proc Natl Acad Sci USA 9:4067–4072.
Dunham NW, Miya TS (1957) A note on a simple apparatus for detecting neurological deficit in rats and mice. J Am Pharm Assoc (Wash) XLVI:5–8.
Eddy NB, Leimbach D (1953) Synthetic analgesic (II): dithienylbutenyl and dithienylbutylamines. J Pharmacol Exp Ther 107:385–396.
Ehrhard PB, Gauter U, Stalder A, Bauer J, Otten U (1993a) Expression of functional trk proto-oncogene in human monocytes. Proc Natl Acad Sci USA 90:5423–5427.
Ehrhard PB, Erb P, Graumann U, Otten U (1993b) Expression of nerve growth factor and nerve growth factor tyrosine kinase Trk in activated CD4-positive T cell clones. Proc Natl Acad Sci USA 90:10981–10984.
Franklin K, Paxinos G (1997) The mouse brain in stereotaxic coordinates. San Diego: Academic.
Frick KM, Price DL, Koliatsos VE, Markowska AL (1997) The effects of nerve growth factor on spatial recent memory in aged rats persist after discontinuation of treatment. J Neurosci 17:2543–2550.
Gonfloni S (1995) Recombinant antibodies as structural probes for neurotrophins. PhD thesis, SISSA.
Gorin PD, Johnson Jr EM (1979) Experimental autoimmune model of nerve growth factor deprivation: effects on developing peripheral sympathetic and sensory neurons. Proc Natl Acad Sci USA 76:5382–5386.
Gorin PD, Johnson Jr EM (1980) Effects of exposure to nerve growth factor antibodies on the developing nervous system of the rat: an experimental autoimmune approach. Dev Biol 80:313–323.
Gustilo MC, Markowska AL, Breckler SJ, Fleischman CA, Price DL, Koliatsos VE (1999) Evidence that nerve growth factor influences recent memory through structural changes in septohippocampal cholinergic neurons. J Comp Neurol 405:491–507.
Haas IG, Wabl M (1983) Immunoglobulin heavy chain binding protein. Nature 306:387–389.
Ibanez CF (1995) Neurotrophic factors: from structure-function studies to designing effective therapeutics. Trends Biotechnol 13:217–227.
Ibanez CF (1998) Emerging themes in structural biology of neurotrophic factors. Trends Neurosci 21:438–444.
Johnson EM, Gorin PD, Brandeis LD, Pearson J (1980) Dorsal root ganglion neurons are destroyed by exposure in utero to maternal antibodies to nerve growth factor. Science 210:916–918.
Korsching S (1986) The role of nerve growth factor in the CNS. Trends Neurosci 9:570–573.
Korsching S, Thoenen H (1983) Nerve growth factor in sympathetic ganglia and corresponding target organs of the rat: correlation with density of sympathetic innervation. Proc Natl Acad Sci USA 80:3513–3516.
Lee K-F, Li E, Huber LJ, Landis SC, Sharpe AH, Chao MV, Jaenisch R (1992) Targeted mutation of the gene encoding the low affinity NGF receptor p75 leads to deficits in the peripheral sensory nervous system. Cell 6:737–749.
Levi-Montalcini R (1952) Effects of mouse tumor transplantation on the nervous system. Ann NY Acad Sci 55:330–343.
Levi-Montalcini R (1987) The nerve growth factor 35 years later. Science 237 1154–1162.
Levi-Montalcini R, Angeletti PU (1966) Immunosympathectomy. Pharmacol Rev 18:619–628.
Levi-Montalcini R, Booker B (1960) Destruction of the sympathetic ganglia in mammals by an antiserum to a nerve growth factor protein. Proc Natl Acad Sci USA 46:384–391.
Levine JD (1998) New directions in pain research: molecules to maladies. Neuron 20:649–654.
Li Y, Holtzman DM, Kromer LF, Kaplan DR, Chua-Couzens J, Clary DO, Knusel B, Mobley WC (1995) Regulation of TrkA and ChAT expression in developing rat basal forebrain: evidence for both exogenous and endogenous NGF regulate differentiation of cholinergic neurons. J Neurosci 15:2888–2905.
Markowska AL, Price D, Koliatsos VE (1996) Selective effects of nerve growth factor on spatial recent memory as assessed by a delayed nonmatching-to-position task in the water maze. J Neurosci 16:3541–3548.
Michel RP, Cruz-Orive LM (1988) Application of the Cavelieri principle and vertical sections method to lung: estimation of volume and pleural surface. J Microsc 150:117–136.
Molnar M, Ruberti F, Cozzari C, Domenici L, Cattaneo A (1997) A critical period for the sensitivity of basal forebrain cholinergic neurons to NGF deprivation. NeuroReport 8:575–579.
Molnar M, Tongiorgi E, Avignone E, Gonfloni S, Ruberti F, Domenici L, Cattaneo A (1998) The effects of anti-nerve growth factor monoclonal antibodies on developing basal forebrain neurons are transient and reversible. Eur J Neurosci 10:3127–3140.
Neuberger MS, Caskey HM, Pettersson S, Williams GT, Surani MA (1989) Isotype exclusion and transgene down-regulation in immunoglobulin-lambda transgenic mice. Nature 338:350–352.
Peterson DA, Dickinson-Anson HA, Leppert JT, Lee KF, Gage FH (1999) Central neuronal loss and behavioral impairment in mice lacking neurotrophin receptor p75. J Comp Neurol 404:1–20.
Pettersson S, Sharpe MJ, Gilmore DR, Surani MA, Neuberger MS (1989) Cellular selection leads to age-dependent and reversible down-regulation of transgenic immunoglobulin light chain genes. Int Immunol 1:509–516.
Piccioli P, Ruberti F, Biocca S, Di Luzio A, Werge TM, Bradbury A, Cattaneo A (1991) Neuroantibodies: molecular cloning of a monoclonal antibody against substance P for the expression in the central nervous system. Proc Natl Acad Sci USA 88:5611–5615.
Piccioli P, Di Luzio A, Amann R, Schuligoi R, Azim Surani M, Donnerer J, Cattaneo A (1995) Neuroantibodies: ectopic expression of a recombinant anti-substance P antibody in the central nervous system of transgenic mice. Neuron 15:373–384.
Rashid K, Van der Zee CEEM, Ross GM, Chapman CA, Stanisz J, Riopelle RJ, Racine RJ, Fahnestock M (1995) A nerve growth factor peptide retards seizure development and inhibits neuronal sprouting in a rat model of epilepsy. Proc Natl Acad Sci USA 92:9495–9499.
Ruberti F, Bradbury A, Cattaneo A (1993) Cloning and expression of an anti-nerve growth factor (NGF) antibody for studies using the neuroantibody approach. Cell Mol Neurobiol 13:559–568.
Ruberti F, Berretta N, Cattaneo A, Cherubini E (1997) NGF antibodies impair long-term depression at the mossy fibre-CA3 synapse in the developing hippocampus. Dev Brain Res 101:295–297.
Ruit KG, Elliott JL, Osborne PA, Yan Q, Snider WD (1992) Selective dependence of mammalian dorsal root ganglion neurons on nerve growth factor during embryonic development. Neuron 8:1–20.
Rylett RJ, Williams LR (1994) Role of neurotrophins in cholinergic-neurone function in the adult and aged CNS. Trends Neurosci 17:486–490.
Seidl K, Erck C, Buchberger A (1998) Evidence for the participation of nerve growth factor and its low-affinity receptor (p75NTR) in the regulation of the myogenic program. J Cell Physiol 176:10–21.
Sendtner M, Holtmann B, Hughes RA (1996) The response of motoneurons to neurotrophins. Neurochem Res 21:831–841.
Shelton DL, Reichardt LF (1984) Expression of the beta-nerve growth factor gene correlates with the density of sympathetic innervation in effector organs. Proc Natl Acad Sci USA 81:7951–7955.
Silos-Santiago I, Molliver DC, Ozaki S, Smeyne RJ, Fagan AM, Barbacid M, Snider WD (1995) Non-TrkA-expressing small DRG neurons are lost in TrkA deficient mice. J Neurosci 15:5929–5942.
Smeyne RJ, Klein R, Schnapp A, Long LK, Bryant S, Lewin A, Lira SA, Barbacid M (1994) Severe sensory and sympathetic neuropathies in mice carrying a disrupted Trk/NGF receptor gene. Nature 368:246–249.
Snider WD (1994) Functions of the neurotrophins during nervous system development: what the knockouts are teaching us. Cell 77:627–638.
Snider WD, McMahon SB (1998) Tackling pain at the source: new ideas about nociceptors. Neuron 20:629–632.
Sterio DC (1984) The unbiased estimation of number and sizes of arbitrary particles using the disector. J Microsc 134:127–136.

Storb U, Pinkert C, Arp B, Engler P, Gollahon K, Manz J, Brady W, Brinster R (1986) Transgenic mice with μ and κ genes encoding anti phosphorylcholine antibodies. J Exp Med 164:627–641.

Torcia M, Bracci-Laudiero L, Lucibello M, Nencioni L, Labardi D, Rubartelli A, Cozzolino F, Aloe L, Garaci E (1996) Nerve growth factor is an autocrine survival factor for memory B lymphocytes. Cell 85:345–356.

Van der Zee CEEM, Lourenssen S, Stanisz J, Diamond J (1995) NGF-deprivation of adult brain results in cholinergic hypofunction and impaired spatial learning behavior. Eur J Neurosci 7:160–168.

Vijayan V (1979) Distribution of cholinergic neurotransmitter enzymes in the hippocampus and the dentate gyrus of the adult and developing mouse. Neuroscience 4:121–137.

Wenzel HJ, Cole TB, Born DE, Schwartzkroin PA, Palmiter RD (1997) Ultrastructural localization of zinc transporter-3 (ZnT-3) to synaptic vesicle membranes within mossy fiber boutons in the hippocampus of mouse and monkey. Proc Natl Acad Sci USA 94:12676–12681.

West MJ (1993) New stereological methods for counting neurons. Neurobiol Aging 14:275–285.

Yamamoto M, Sobue G, Yamamoto K, Terao S, Mitsuma T (1996) Expression of mRNAs for neurotrophic factors (NGF, BDNF, NT-3, and GDNF) and their receptors (p75NGFR, trkA, trkB, and trkC) in the adult human peripheral nervous system and non neural tissue. Neurochem Res 2:929–938.